Study of rhombohedral tricalcium phosphate in hexagonal crystal structure family on the sample prepared by the sol-gel route and the effect of calcination temperature

J. Ady[1,2], S. D. A. Ariska[1], D. I. Rudyardjo[1,2], S. Anindriya[2]*
[1]*Airlangga University, Faculty of Science and Technology, Department of Physics, 60115 Surabaya, Indonesia*
[2]*Airlangga University, Faculty of Science and Technology, Biomedical Engineering Study Program, 60115 Surabaya, Indonesia*

Abstract

The effect of the calcination temperature at 800 and 1000 °C on the stable formation of the tricalcium phosphate with rhombohedral structure in the system of the hexagonal crystal family was determined, while its precursor was made from limestone obtained from nature in the Lumajang district, Indonesia. The rhombohedral tricalcium phosphate samples were prepared by sol-gel routine, then examined by several tests, such as, Fourie transform infrared spectroscopy to study the deficiency of -OH, X-ray diffraction test to study the microstructure of the tricalcium phosphate with the rhombohedral structure in a hexagonal crystal system, differential scanning calorimetry and thermogravimetry tests to study thermal characteristics, scanning electron microscopy and energy dispersive spectroscopy to study the surface topography and to obtain the atomic ratio Ca/P ~1.5. Finally, the UV-vis test found the optical energy gap, E_g, from ~5.34 to ~5.41 eV for the sample calcined at 800 °C and E_g ~5.19 to ~5.21 eV at 1000 °C.
Keywords: tricalcium phosphate, sol-gel, temperature, rhombohedral, research, structure.

INTRODUCTION

In crystallography, there are six crystal families, one is the hexagonal crystal family, which includes two crystal systems (hexagonal and trigonal) and two lattice systems (hexagonal and rhombohedral). Meanwhile, the rhombohedral crystal structure is depicted inside the hexagonal crystal system. Tricalcium phosphate is one of several ceramic compounds derived from hydroxyapatite that has a stable crystal structure in a hexagonal system. Tricalcium phosphate (TCP) is an attractive material or biomaterial such as bone phosphate of lime (BPL) with low solubility in the white solid form. In the general commercial product, TCP is produced by treating hydroxyapatite (HA_p) with phosphoric acid and slaked lime. TCP or BPL have three recognized polymorphs, namely: 1) rhombohedral (β-TCP), 2) monoclinic (α-TCP), and 3) hexagonal (α'-TCP) forms. The rhombohedral TCP has a crystal denser than monoclinic or hexagonal TCP in its own stable temperature, however, are less dense at high temperature. They are potentially used in medicine, such as for bone substitutes either in dense or porous forms [1-3]. The melting point of TCP is about ~1670 °C [4], and it was indicated the effective sintering temperature at about ~1113 °C when it was calculated by using 2/3 of the melting temperature [5, 6]. The solid phases of TCP in three existing forms namely β-, α-, and α'-TCP always made from low, near, and same sintering temperatures [7].

There are several methods of the synthesis of polymorphic tricalcium phosphates; among others, they are prepared by solid-state reaction and wet methods or wet chemical precipitation (sol-gel) route [8-12]. The novelty of this research is to provide raw material for artificial bone based on tricalcium phosphate with a rhombohedral crystal structure by utilizing natural limestone available in Indonesia. In several previous tricalcium phosphate studies using the sol-gel technique, the $CaCO_3$ compounds have been used as a precursor in the sol-gel route, but many studies use fabricated $CaCO_3$ compounds with varying levels of purity. Meanwhile, the use of $CaCO_3$ compounds from natural materials is rarely carried out in similar studies. Therefore, the novelty of this study is related to: 1) the use of a novel $CaCO_3$ material as a precursor in the sol-gel route for the sample preparation of tricalcium phosphate derived from the mineral limestone (natural raw material) in the Lumajang region, East Java, Indonesia; 2) this research study focused on the microstructure of tricalcium phosphate in the rhombohedral crystal system which is a family of hexagonal crystal structure with the level of stability of the crystal structure affected by heating temperature; and 3) the search for the potential use of the novel materials of $CaCO_3$ as an artificial bone bioceramic derived by a limestone mineral in Lumajang with the rhombohedral system crystal characteristics. In this focus, the rhombohedral tricalcium phosphate was prepared from limestone ($CaCO_3$) that was obtained from nature in the Lumajang district, with the use

**jan-a@fst.unair.ac.id*
https://orcid.org/0000-0002-5408-580X

of a wet method in sol-gel routine, and after that influenced by calcination temperature at 800 and 1000 °C. The sol-gel technique was preferred in this research due to the simplicity of the method regarding the preparation handling and because it provides a nanometer scale for the crystal size. In other words, this preparation technique always produces a finely powdered sample in the nanosized form [13, 14]. Previously, there are several appropriate tests to justify the rhombohedral tricalcium phosphate in the hexagonal crystal structure form already formed by sol-gel technique, such as: 1) FTIR test: it was used to study the functional group [15-17], especially for deficiency of the hydroxyl functional group (-OH) analysis when temperatures of 800 and 1000 °C were applied on sample; 2) XRD test [18-20]: it was used to analyze the lattice system of crystal, through studies of the crystallite size, strain, dislocation density, crystallinity, and the preferential plane of the rhombohedral tricalcium phosphate in the hexagonal crystal structure; 3) DSC-TGA test [21, 22]: it was used to analyze the thermal responses including information of specific heat capacity, mass reduction, enthalpy of fusion and melting; 4) SEM-EDX test [23-27]: it was used to analyze the surface morphology and the atomic ratio Ca/P ~1.5; and finally, 5) UV-vis test [28, 29]: it was used to analyze the optical energy gap (E_g) of the rhombohedral tricalcium phosphate sample with Tauc formula to determine the E_g value.

This study is relevant for giving information about the effect of temperature, exactly at 800 and 1000 °C for stable structure formation of tricalcium phosphate sample in the hexagonal crystal system through a particular study, when the sample was prepared by a sol-gel routine with the use of a limestone precursor obtained from Indonesia. Therefore, the aim of this study is to provide information on temperature leverage as a reinforcing parameter to improve the microstructure of the tricalcium phosphate with rhombohedral structure in a hexagonal crystal system, which is prepared by a sol-gel route and when the effects of temperature at 800 and 1000 °C are applied to this sample, from its gel to the dry phases. Moreover, some parameters of interest were studied by using several examinations, such as looking for the lattice plane of the rhombohedral tricalcium phosphate in the hexagonal crystal structure through its study from XRD results for the determination of the crystallite size, strain, dislocation density, and the crystallinity degree. Subsequently, a functional group of the rhombohedral tricalcium phosphate sample was studied from FTIR results and then studied to find the atomic ratio and their profile surfaces through analysis of SEM-EDX results. Previously, the DSC-TGA thermograms were used to study the specific heat capacity, mass reduction, fusion and melting enthalpies. Finally, the optical energy gap was studied by using the UV-vis result to provide information about thermal characteristics as an insulator.

EXPERIMENTAL

Preparation of rhombohedral tricalcium phosphate samples: the sample was prepared by sol-gel route with the wet reaction method. First, the calcium oxide (CaO) was made from limestone ($CaCO_3$) obtained from nature in the Lumajang district, Indonesia, with a calcination technique at 1100 °C in a laboratory furnace (tabletop-type vertical muffle furnace) for 3 h. Second, the calcium oxide was mixed with water to produce the calcium hydroxide [$Ca(OH)_2$]. Third, the sol-gel route was conducted to find the rhombohedral tricalcium phosphate or calcium and hydroxyl deficiencies in hydroxyapatite form with a Ca/P ratio of ~1.5: i) hydrolysis step: mixing 0.6 M water with 1.6 M of $Ca(OH)_2$ and 1.2 M of H_3PO_4 (ACS reagent, ≥85 wt% in water) using a hot plate magnetic stirrer for 2 h; ii) condensation step: dropping the ethanol into the previous solution that was produced by the hydrolysis step and keep going to mix using the hot plate magnetic stirrer for 15 to 20 h [30-32]; iii) aging step: the gel form of the sample produced by condensation step in the sol-gel route was aged for 20 h at room temperature (~27 °C); iv) drying step: the fine powder of the rhombohedral tricalcium phosphate sample was obtained when its gel form was heated at 800 and 1000 °C.

Examinations of the rhombohedral tricalcium phosphate samples: there were several types of tests used for sample analysis, such as X-ray diffraction analysis (XRD, XPert MPD, Philips; 2θ range: 20-80°, step size: 0.017°, scan step time: 10.15 s), Fourier transform infrared spectroscopy (FTIR, IRPrestige 21, Shimadzu; wavenumber range: 4000-400 cm^{-1}, resolution: ~4 cm^{-1}, mirror speed: ~2.8 mm/s, total of ~10 scans), scanning electron microscopy-energy dispersive X-ray spectroscopy (SEM-EDX, Inspect-S50, FEI), differential scanning calorimetry-thermogravimetric analysis (DSC-TGA, STA PT 1600, Linseiss; temperature range: 27 to 995 °C, heating rate: 25 °C.min^{-1}, atmosphere: air), and ultraviolet-visible spectroscopy (UV-vis, UV-1800, Shimadzu; wavelength range: 190 to 800 nm, scan speed: fast, sampling interval: 0.5 nm). 1) FTIR: this test examined the hydroxyl functional group deficiency of hydroxyapatite compound [$Ca_5(PO_4)_3.(OH)$] that became tricalcium phosphate compound [$Ca_3(PO_4)_2$]. In this effort, the scan parameters were analyzed by using the standardized points of the angular frequency in all spectrum obtained from FTIR on the integrated transmittance count and wavenumber range, to study their type of vibration, where every type of vibration was studied to define the kind of the functional group of -OH, $-PO_4^-$, and $-PO_4^{3-}$. 2) SEM-EDX: this test examined the surface morphology and atomic ratio of the rhombohedral tricalcium phosphate sample, Ca/P ~1.5. In this effort, the step line of the scanning of SEM was used to define the surface morphology of the tricalcium phosphate sample. Meanwhile, the integrated intensity count and spread of electron in the energy level was defined to find the atomic ratio of the tricalcium phosphate sample. 3) XRD: this test examined the crystal system of the rhombohedral tricalcium phosphate by determining some inherent parameters, such as the study of the crystal lattice system which included the crystallite size, strain,

dislocation density, crystallinity, and the preferential plane orientation of the rhombohedral crystal structure in the hexagonal crystal structure. In this effort, every data obtained from XRD scan parameters on the integrated intensity count and full-width at half maximum (FWHM) were analyzed by using the Gaussian method. 4) DSC-TGA: this test examined the thermal responses through the study of some inherent parameters of rhombohedral tricalcium phosphate, such as analysis of the heat flow, specific heat capacity, change of mass, enthalpy of crystallization and fusion reactions via the endothermic and exothermic process. In this effort, the results of the thermogram on the integrated heat flow and time/temperature obtained from DSC-TGA were used to define the thermal parameters, such as heat capacity, mass reduction, enthalpy of fusion and melting quantities. 5) UV-vis: this test examined the optical energy gap of the rhombohedral tricalcium phosphate using Tauc's equation [33, 34]. In this effort, every data obtained from UV-vis spectra were plotted in the absorbance and wavelength, and this curve was used to define the optical energy gap of the tricalcium phosphate sample by using the Tauc plot approach.

RESULTS AND DISCUSSION

FTIR data analysis for rhombohedral tricalcium phosphate functional group: the functional group information of rhombohedral tricalcium phosphate in the hexagonal crystal structure was confirmed by using data analysis from the FTIR test result, where, deficiency of the hydroxyl functional group (-OH) was obtained for samples calcined at 800 and 1000 °C. The wavenumber of -OH was indicated to occur at the point ~3446.6 cm^{-1} with a bit of existence characteristic of transmittance value or big value of absorbance appeared, such as shown in Fig. 1a. In the other words, this indicated that a low vibration occurred with a weak angular frequency for samples calcined at 800 and 1000 °C. The FTIR spectra, such as shown in Fig. 1a, indicated a change from $Ca(OH)_2$ to $Ca_3(PO_4)_2$. Therefore, these FTIR spectra denoted that the rhombohedral tricalcium phosphate effectively was formed by temperature effect at 800 and 1000 °C. Meanwhile, their anion of the functional group of orthophosphate (PO_4^{3-}) was confirmed as asymmetric bending (~566.6 and ~608.9 cm^{-1}) or

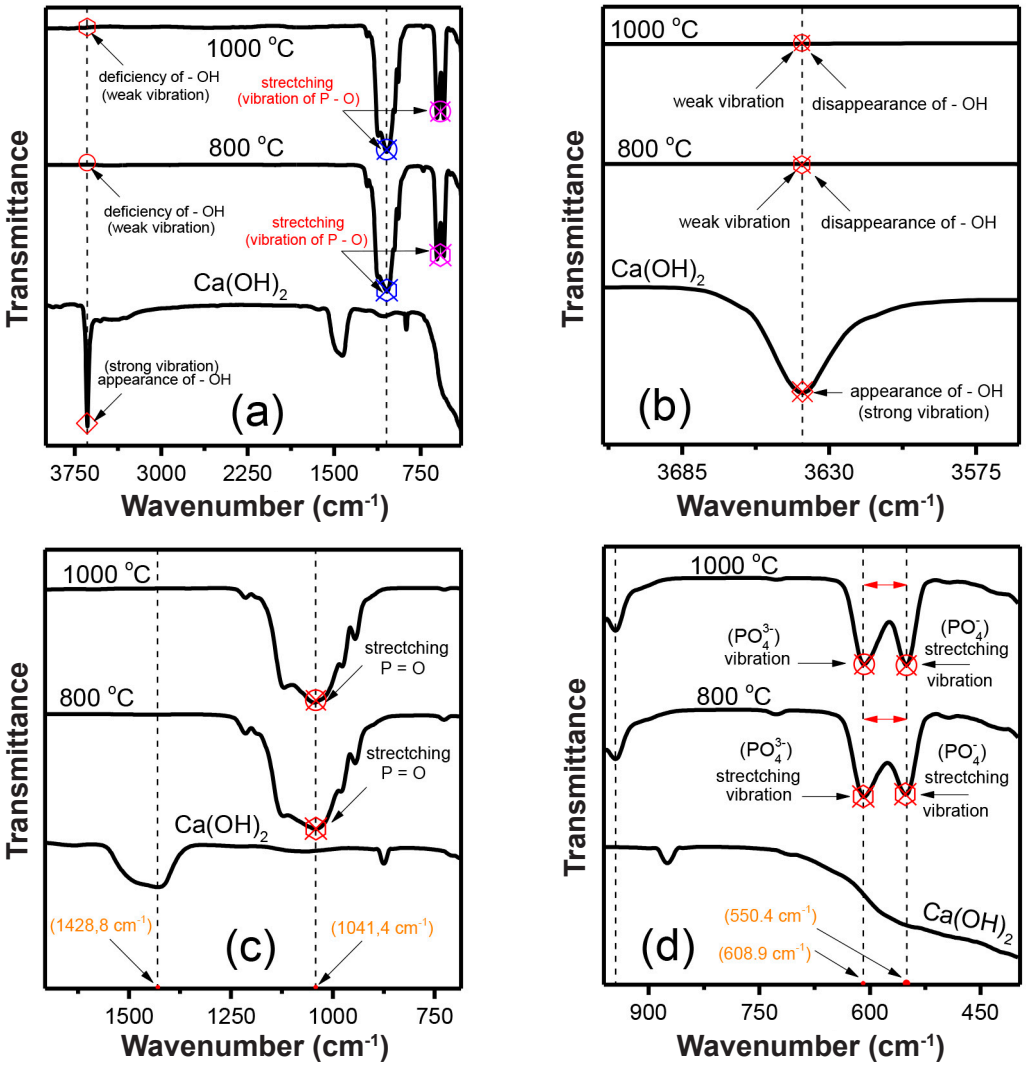

Figure 1: FTIR spectra of samples over the entire range (a) and for specific ranges (b-d) of tested wavenumber.

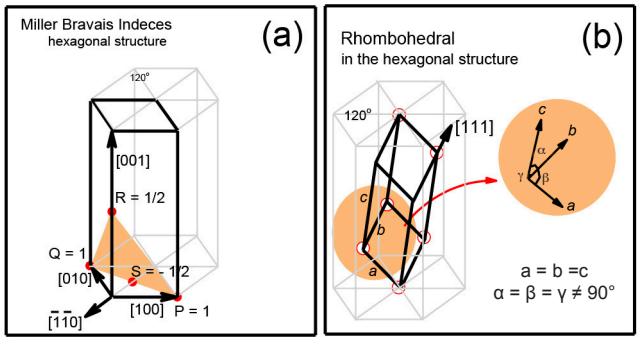

Figure 2: Schematics showing Miller indices (a) and rhombohedral structure (b) in the hexagonal structure.

asymmetric stretching (~1041.4, ~962.4, and ~900.1 cm^{-1}) and with strong frequency vibration value. Moreover, the anion functional group of PO_4^- was confirmed to occur at the point ~550.4 cm^{-1}. Particularly, all FTIR spectra for these samples with the specific wavenumber and transmitted values are shown in Figs. 1b to 1d.

XRD data analysis for rhombohedral tricalcium phosphate in the hexagonal crystal structure: several analyses were conducted by using the XRD results to reveal the crystalline features of the rhombohedral tricalcium phosphate samples in the hexagonal crystal structure, as follows.

Miller indices (hkl) and constant lattice plane determinations for the crystalline samples: lattice planes'

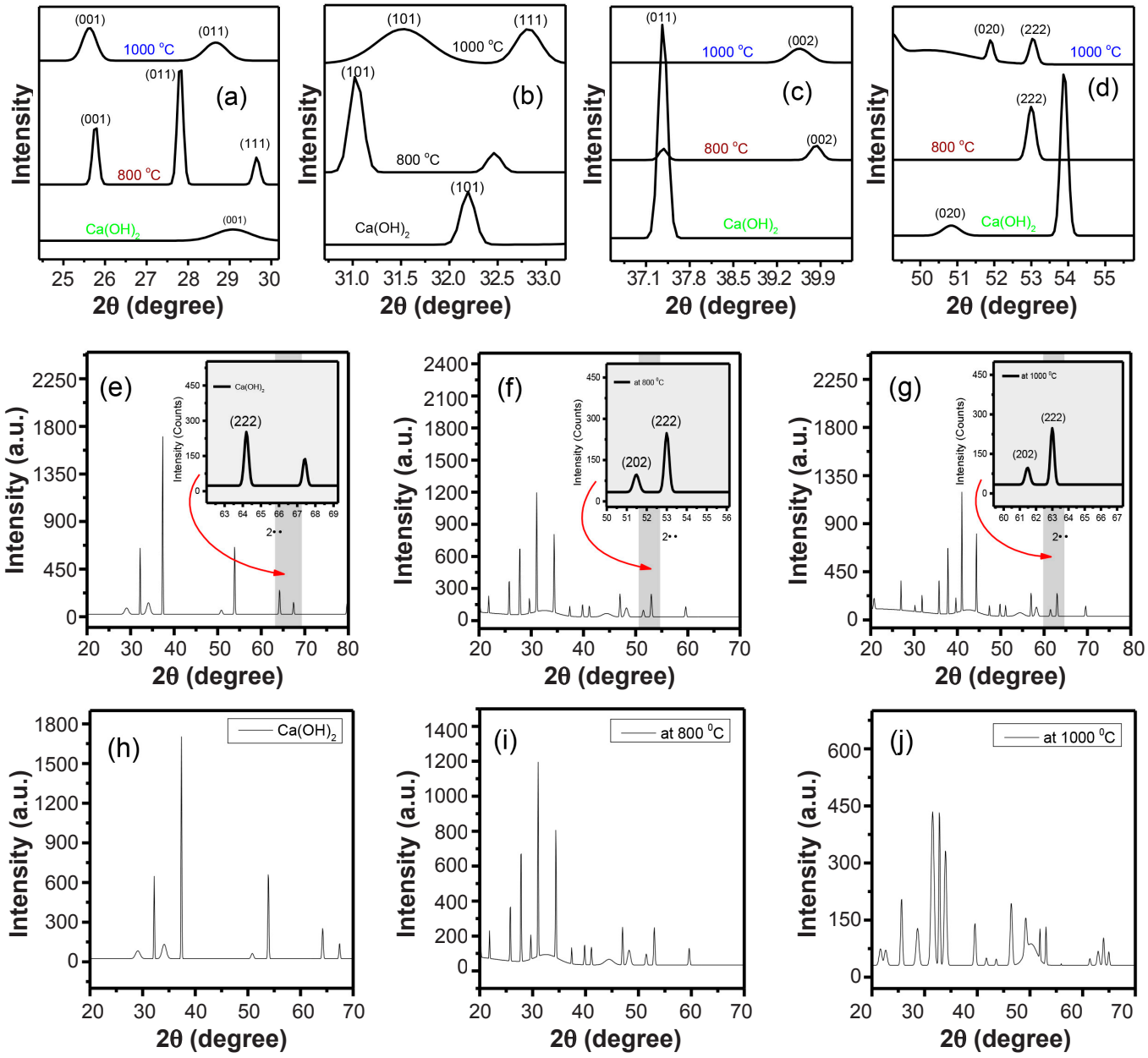

Figure 3: Refinement of the XRD patterns for combined curves of samples at Bragg's angle interval of: a) 25° to 30°; b) 30° to 33°; c) 37° to 40°; and d) 50° to 55°. Diffractograms from 20° to 80° for: e) $Ca(OH)_2$; f) sample heated at 800 °C; and g) sample heated at 1000 °C. Gaussian fitted diffractograms for: h) $Ca(OH)_2$; i) sample heated at 800 °C; and j) sample heated at 1000 °C.

family of the rhombohedral structure of tricalcium phosphate is given by particular Bravais lattice defined by three integers h, k, and l, and denoted as Miller indices with notation (hkl). However, with hexagonal and rhombohedral lattice systems, it is possible to use the Bravais-Miller lattice system, which uses four indices h, k, i, and l or with notation (hkil) that obey the constraint [35, 36]:

$$h + k + i = 0 \qquad (A)$$

where h, k, and l define the Miller indices and i is a redundant index. As follows, the interplanar spacing (d_{hkl}) for the hexagonal system is given by:

$$d_{hkl} = \frac{a}{\sqrt{\frac{4}{3}(h^2+k^2+h.k)+\frac{a^2}{c^2}l^2}} \qquad (B)$$

where a and c are defined as lattice constants and d_{hkl} is corresponding with the crystallite size (D), peak broadening (β), and crystallite strain (ε) parameters. Particularly, D can be determined by using the Scherrer equation and Williamson-Hall plot method [37-39]. Therefore, the Miller indices and lattice constants of the rhombohedral tricalcium phosphate in the hexagonal crystal structure were calculated by using Eqs. A and B. Previously, the XRD pattern obtained was showing the specific peaks of the crystal and amorphous patterns. By means of peak refinement with the Gaussian distribution method in the software used, it was found the specific peak values with Miller indices (001) as a lattice plane orientation for a hexagonal crystal structure with 3-fold symmetry, such as shown in Fig. 2a. Meanwhile, the Miller indices (011) and (111) were described particularly for rhombohedral in the hexagonal crystal structure, as shown schematically in Fig. 2b [40].

The Miller indices of the rhombohedral tricalcium phosphate in the hexagonal crystal structure appeared in the XRD pattern of this sample, as shown particularly for specific Bragg angles in Figs. 3a to 3d. The Miller indices (001) appeared at 2θ ~25.76° and ~25.61° for samples heated at 800 and 1000 °C, respectively, whereas, for $Ca(OH)_2$ they appeared at 2θ ~29.07°. The peak (001) looked like shifted when the temperature at 800 and 1000 °C was applied if compared with the peak (001) of $Ca(OH)_2$. In the same way, Miller indices for rhombohedral lattice planes (011) and (111) were defined at 2θ ~27.78° and ~29.66° for the sample heated at 800 °C. Subsequently, for (011) and (111) of the sample heated at 1000 °C, they were confirmed sequentially at 2θ ~31.52° and ~32.81°. Overall, the Miller indices of rhombohedral tricalcium phosphate in the hexagonal crystal structure were found, such as shown in the particular Bragg angle in Figs. 3a to 3d. Meanwhile, the X-ray diffractograms for $Ca(OH)_2$ and samples heated at 800 and 1000 °C from 20° to 80° are shown in Figs. 3e to 3g and the Gaussian fitted diffractograms are shown in Figs. 3h to 3j. Entirely, the specific Miller indices corresponded with the interplanar spacing from the rhombohedral tricalcium phosphate sample, and according to Eq. B, they were appropriated with the lattice plane orientation to the hexagonal crystal structure model shown in Fig. 4.

Peak broadening, crystallite size, strain, and dislocation density of rhombohedral tricalcium phosphate: in 1918 Scherrer derived a formula relating the mean of the volume average of crystallite size, D, of a powder to the broadening, β, of its powder diffraction peaks ignoring other effects such as strain [41, 42], as described by:

$$D(\beta,\theta) = \frac{K.\lambda}{\beta.\cos\theta} \qquad (C)$$

where θ is the usual Bragg angle, λ is the radiation wavelength, and K is a constant that depends on the assumption in the theory. Particularly, the refinements of X-ray patterns for the samples $Ca(OH)_2$, heated at 800 and 1000 °C are shown in Figs. 5a to 5c. The refinement curves obtained by using the Gaussian method were used to determine several corresponding parameters in Eqs. C and D, such as a crystallite size D(β,θ), broadening β, and strain ε. The formulation in Eq. D was attributed to G. K. Williamson and his student, W. H. Hall. Subsequently, by

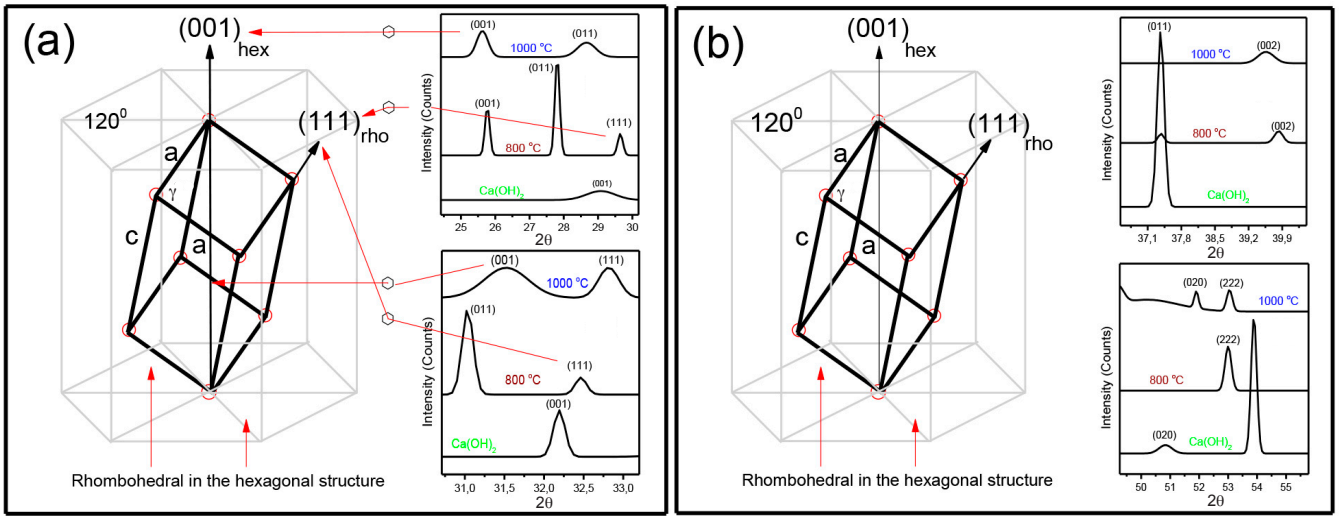

Figure 4: Representation of rhombohedral Miller indices in the 2θ range from: a) ~24.4° to ~33.2°; and b) ~36.5° to 55.6°.

using a software (Origin Pro) approximation to determine the FWHM values that varied quite differently with respect to Bragg angle θ, the crystallite broadening parameter β was found. These all parameters found were related to the specific Miller indices for rhombohedral tricalcium phosphate in the hexagonal crystal structure described previously.

$$\beta.\cos\theta = 4\varepsilon.\sin\theta + \frac{K.\lambda}{D(\beta,\theta)} \qquad (D)$$

Particularly, Figs. 6a to 6c denote specific Miller indices (001) at different Bragg angle values for sample $Ca(OH)_2$, heated at 800 and at 1000 °C. The Miller indices (001) is one of three lattice plane orientations for hexagonal crystal structure, with the rhombohedral crystal structure inside with 3-fold symmetry, [100], [010], and [110], such as shown in Fig. 2. The quantities of several parameters are shown in Table I, where the crystallite size D, strain ε, and dislocation density δ values were calculated by using Eqs. A and D. Previously, the data were plotted (Fig. 5d), after fitted by the linear equation in the curve βcosθ vs. 4sinθ, and then from the linear regression the slope and intercept values were found (Fig. 6d). The curve slope gave the crystallite strain value and from curve intercept the crystallite size value was found. All values of the crystallite size D, strain ε, and dislocation density δ of the rhombohedral tricalcium phosphate sample are displayed in Table I. The slope of linear regression in Fig. 6d tended to decrease with the crystallite strain, resulting in negative values for the samples $Ca(OH)_2$ and heated at 800 °C. Conversely, for the sample heated at 1000 °C, it tended to increase with the crystallite strain and had a positive value. Consequently, the crystallite strain was proportional to the crystallite dislocation density value, however, it was reciprocal to the crystallite size value.

SEM-EDX analysis for rhombohedral tricalcium phosphate in the hexagonal crystal structure: the SEM-EDX results for two samples that are comparable, those heated at 800 and 1000 °C, are shown. Previously, the surface profile of samples calcined at 800 and 1000 °C looked different from one another, as shown in Figs. 7a and 7b. Both seemed like a white cloud, however, the sample calcined at 1000 °C looked denser than the sample calcined at 800 °C. This indicated that the increase in temperature from 800 to 1000 °C influenced the grain size of the rhombohedral tricalcium phosphate sample which became denser. Meanwhile, the quantities

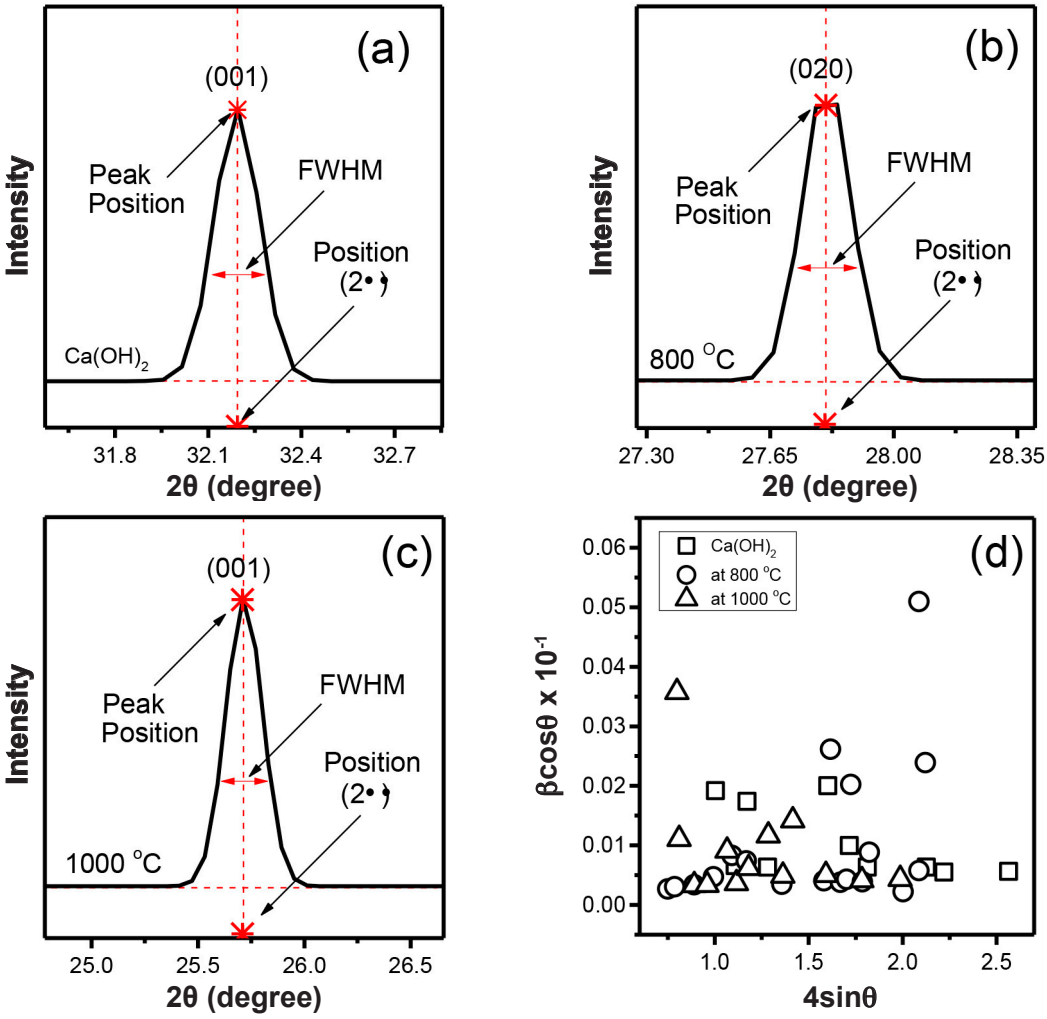

Figure 5: XRD peak at particular Bragg's angle and Miller indices for $Ca(OH)_2$ (a), sample heated at 800 °C (b) and at 1000 °C (c), and W-H plot, βcosθ versus 4sinθ (d).

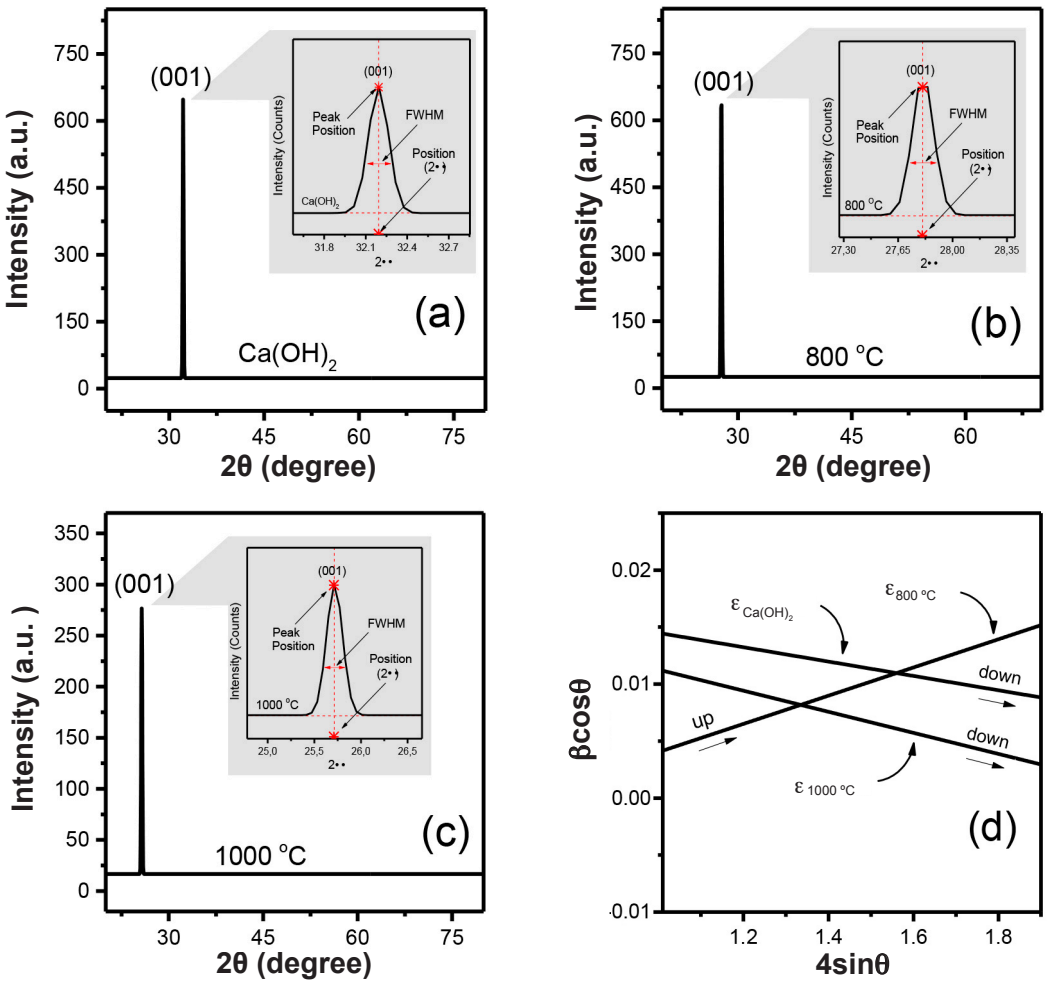

Figure 6: XRD peak for the specific Miller indices at (001) for $Ca(OH)_2$ (a), sample heated at 800 °C (b) and at 1000 °C (c), and W-H plot for crystallite strain determinations, $\varepsilon_{Ca(OH)2}$, $\varepsilon_{800°C}$, and $\varepsilon_{1000°C}$.

Table I - Crystallite size (D), strain (ε), dislocation density (δ), and crystallinity of samples calculated by using the XRD data.

Sample	D (nm)	ε	δ (nm^{-2})	Crystallinity (%)
$Ca(OH)_2$	69.3	-0.001±0.003	0.21	65.7
Heated at 800 °C	86.7	0.012±0.006	0.83	71.3
Heated at 1000 °C	73.0	-0.008±0.007	0.18	69.1

of elements in the samples of rhombohedral tricalcium phosphate obtained by EDX analysis are shown in Table II. The atomic ratio Ca/P ~1.3 and mass ratio Ca/P ~1.4 of the sample heated at 800 °C were found whilst for the sample heated at 1000 °C the atomic ratio Ca/P ~1.43 and mass ratio Ca/P ~1.7. Therefore, the nearly rhombohedral tricalcium sample was formed with a chemical formula β-$Ca_3(PO_4)_2$ or β-TCP for both samples calcined at 800 and 1000 °C. In other words, the high calcination temperature, particularly at 800 and 1000 °C, was effective to form the rhombohedral tricalcium phosphate, which previously was proven by XRD analysis in this study.

DSC-TGA analysis of gel sample: the thermal analysis of the gel sample was examined by using the DSC-TGA equipment and it was set up looking for the effective calcination temperature. 800 and 1000 °C were chosen to conduct different treatments on the sample to obtain the rhombohedral tricalcium phosphate. However, these temperatures had to be compared with other references, before being used as an effect in the sample. The recorded thermogram of DSC plotted as heat flow versus temperature and TGA curve are shown in Fig. 8. On a DSC curve, endothermic and exothermic processes occur that can be described by the enthalpy changes during glass transition, melting, and crystallization. Simultaneously, the mass reduction with temperature (TGA curve) can be obtained. In particular temperature ranges of the thermogram of DSC-TGA gave the endothermic and exothermic process,

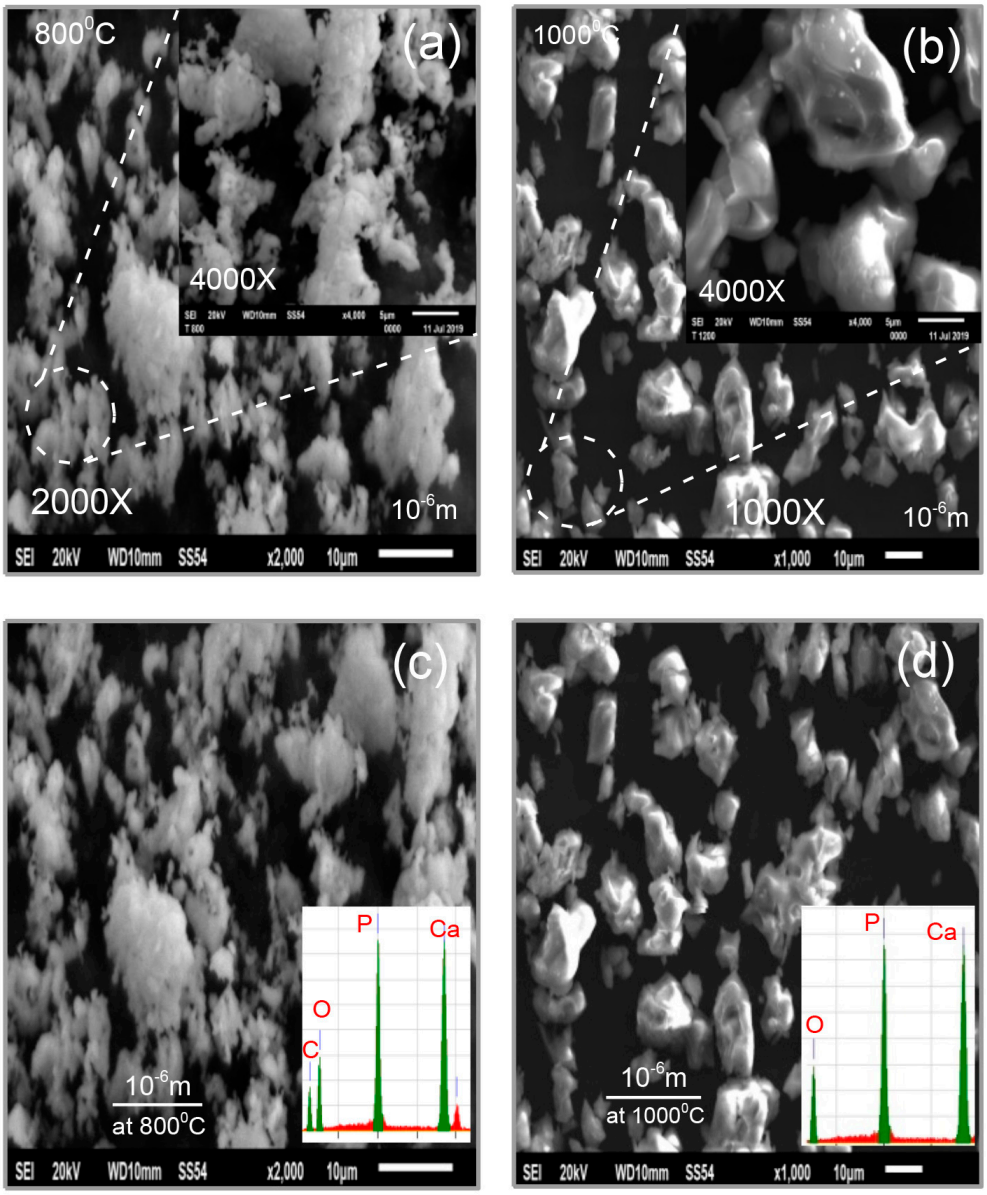

Figure 7: SEM images of samples heated at 800 °C (a,c) and 1000 °C (b,d); EDX spectra are included in (c,d).

Table II - Quantities of elements of samples obtained from the EDX test.

Element	Mass (%)	Atomic (%)	Error (%)
Sample heated at 800 °C			
O	36.08	39.68	0.30
P	14.13	7.02	0.06
Ca	19.72	8.98	0.10
C	30.07	44.32	0.08
Sample heated at 1000 °C			
O	41.42	53.32	0.27
P	17.08	11.12	0.06
Ca	29.86	15.87	0.09
C	11.64	19.69	0.09

denoted by the peak-to-peak shifting. In Fig. 8a, the initial peak appeared for an endothermic reaction in the DSC and TGA thermogram curves at about 60 to 128 °C, and an exothermic reaction occurred at about 130 to 159 °C. After that, sequentially in the temperature range from 146 to 184 °C for endothermic reaction and ~190 to ~240 °C for exothermic process occurred (Fig. 8b). Furthermore, at about 354 to 402 °C for endothermic reaction and about 406 to 460 °C for exothermic process occurred (Fig. 8c). Finally, in the temperature range from about 614 to 748 °C for exothermic reaction and about 758 to 855 °C for endothermic process occurred (Fig. 8d). Therefore, based on these results and compared with appropriate references related to the topic, the study of rhombohedral tricalcium phosphate in hexagonal crystal structure was influenced by the chosen temperatures of 800 and 1000 °C, when the sample was previously prepared by the sol-gel route. Meanwhile, the

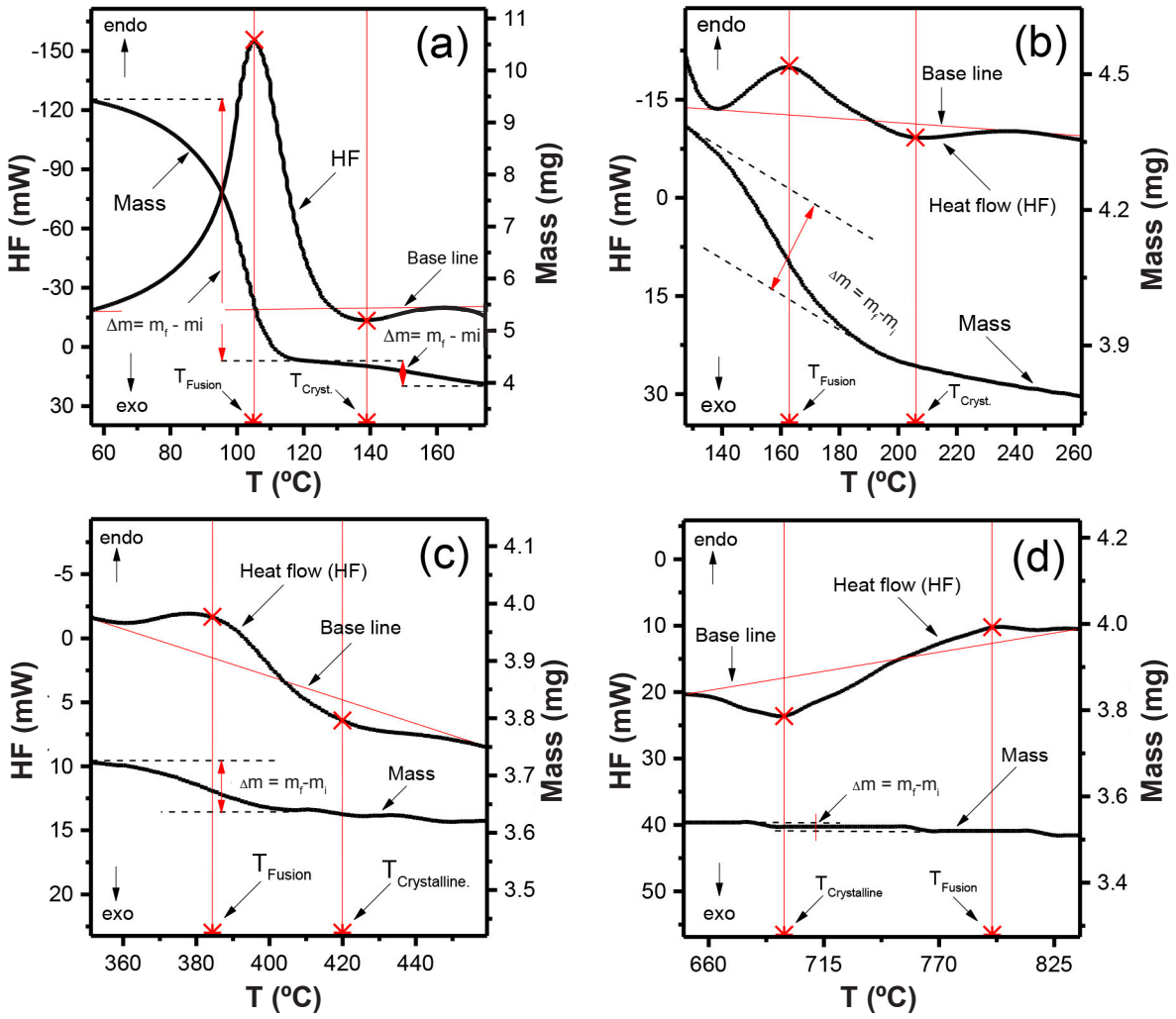

Figure 8: DSC-TGA thermograms of gel sample in the specific temperature ranges.

Table III - Results of melting point (T_i and T_f), enthalpy of fusion (ΔH_F), enthalpy of crystallization (ΔH_C), and specific heat capacity (C_P) of gel sample.

T_i (°C)	T_f (°C)	ΔH_F ($J.g^{-1}$)	ΔH_C ($J.g^{-1}$)	C_P ($J.g^{-1}.°C^{-1}$)
91.12	131.13	1290.34	42.45	4.43
359.06	465.76	57.87	27.06	0.58
617.28	653.15	8.01	123.13	12.89
937.87	960.15	8.78	10.98	6.21

values of melting point, enthalpy of fusion, enthalpy of crystallization, and specific heat capacity of the samples treated at 800 and 1000 °C were calculated by using the DSC-TGA results and are shown in Table III.

Figs. 9a and 9c show the melting and crystallization points as a function of time or temperature. Every endothermic peak is the point of melting or fusion. Otherwise, each exothermic peak is a point of crystallization, such as denoted by the red sign in Figs. 9a and 9c, whilst each endothermic peak area is the quantity of enthalpy of fusion or melting, and each exothermic peak area is a quantity of enthalpy of crystallization, as denoted by hatched areas in Fig. 9b. For a specific mass reduction in the TGA curve at the temperature range from ~27 to ~190 °C showed that the DTG (derivative of TGA) curve was instantaneously shifted following the mass change (Fig. 9d). This result indicated the crystalline structure of the sample was changed as a function of temperature and the chemical bond changed when heat flowed in (absorbed by the endothermic process) or out (released by the exothermic process) [43, 44]. Table III shows the results of initial, T_i, and final, T_f, melting or fusion temperatures, enthalpy of fusion, ΔH_F, and crystallization, ΔH_C, and specific heat capacity, C_P. These results indicated that the gel phase of the rhombohedral tricalcium phosphate sample became a dry powder, and justified the temperature range from ~937.87 to ~960.15 °C. Therefore, based on this analysis, the temperatures chosen were 800 and 1000 °C in this work and then their effects on the rhombohedral tricalcium phosphate inside the hexagonal crystal structure were studied.

UV-vis analysis for rhombohedral tricalcium phosphate in the hexagonal crystal structure: analysis of the optical

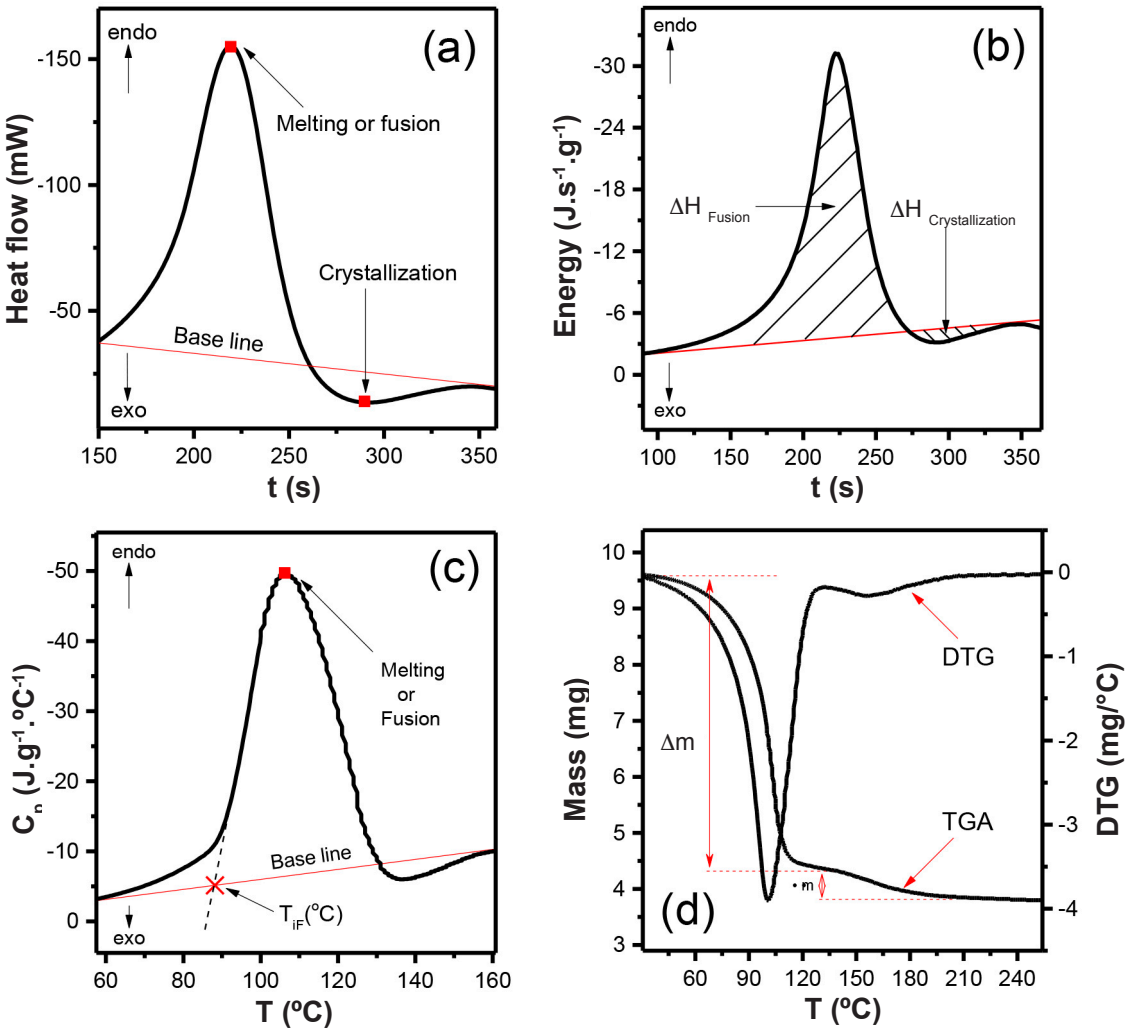

Figure 9: Curves of heat flow versus time (a), energy versus time (b), C_p versus temperature (c), and TGA and DTG thermograms (d).

properties of the rhombohedral tricalcium phosphate sample in this work was conducted by using UV-vis spectroscopy. This is one of the important characterization techniques to understand the interaction between the matrix and filler inside a synthesized sample and to analyze the effects to enhance the properties of a composite sample. Therefore, this technique was used in this work to look for the optical band gap of the rhombohedral tricalcium phosphate sample. In the beginning, the UV-vis spectroscopy gave the absorption spectra of samples in duplicate for sample calcined at 800 °C (Figs. 10a and 10b) and at 1000 °C (Figs. 10c and 10d). The optical band gap of rhombohedral tricalcium phosphate samples was found by using the Tauc plot and using Eq. E:

$$(\alpha.h.\nu)^{\gamma} = A(h.\nu - E_g) \qquad (E)$$

where α is the absorption coefficient, h is Planck's constant, ν is the frequency of the incident photon, A is a proportionality constant determined by the index of refraction, and E_g is the optical band gap energy. The important term is the exponent γ, which denotes the nature of the electronic transition. There are some terms for the exponent γ in Eq. E; when γ=2, it is a direct allowed transition, when γ=1/2, it is an indirect allowed transition, when γ=2/3, it is a direct forbidden transition, and when γ=1/3, it is an indirect forbidden transition. However, typically, the allowed transitions are dominated by the basic absorption processes giving either direct or indirect transitions [45, 46]. Thus, the basic procedure for Tauc analysis is to acquire the absorbance data of a sample from UV-vis spectral information, as shown in Fig. 10, where the band gap transition energy is defined. By plotting the $(\alpha h\nu)^2$ versus hν (considering γ=2 in Eq. E), a graph such as those shown in the insets of Fig. 10 is obtained. Extrapolation of the linear curve of the plot onto the x-axis gave the optical band gap or edge energy, just as Tauc's equation was used in 1968 to calculate the absorption edge or band gap energy [47, 48].

By twice plotting curves of the $(\alpha h\nu)^2$ versus (hν) for the sample calcined at 800 °C, the optical band gap energy (E_g) was found to be ~5.34 and ~5.41 eV (Figs. 10a and 10b). Meanwhile, for the sample calcined at 1000 °C, the determined E_g values were ~5.19 and ~5.21 eV (Figs. 10c and 10d). Therefore, rhombohedral tricalcium phosphate samples are responsive under UV-vis light. However, it is still unclear to define that it can behave as a photocatalyst under UV-vis

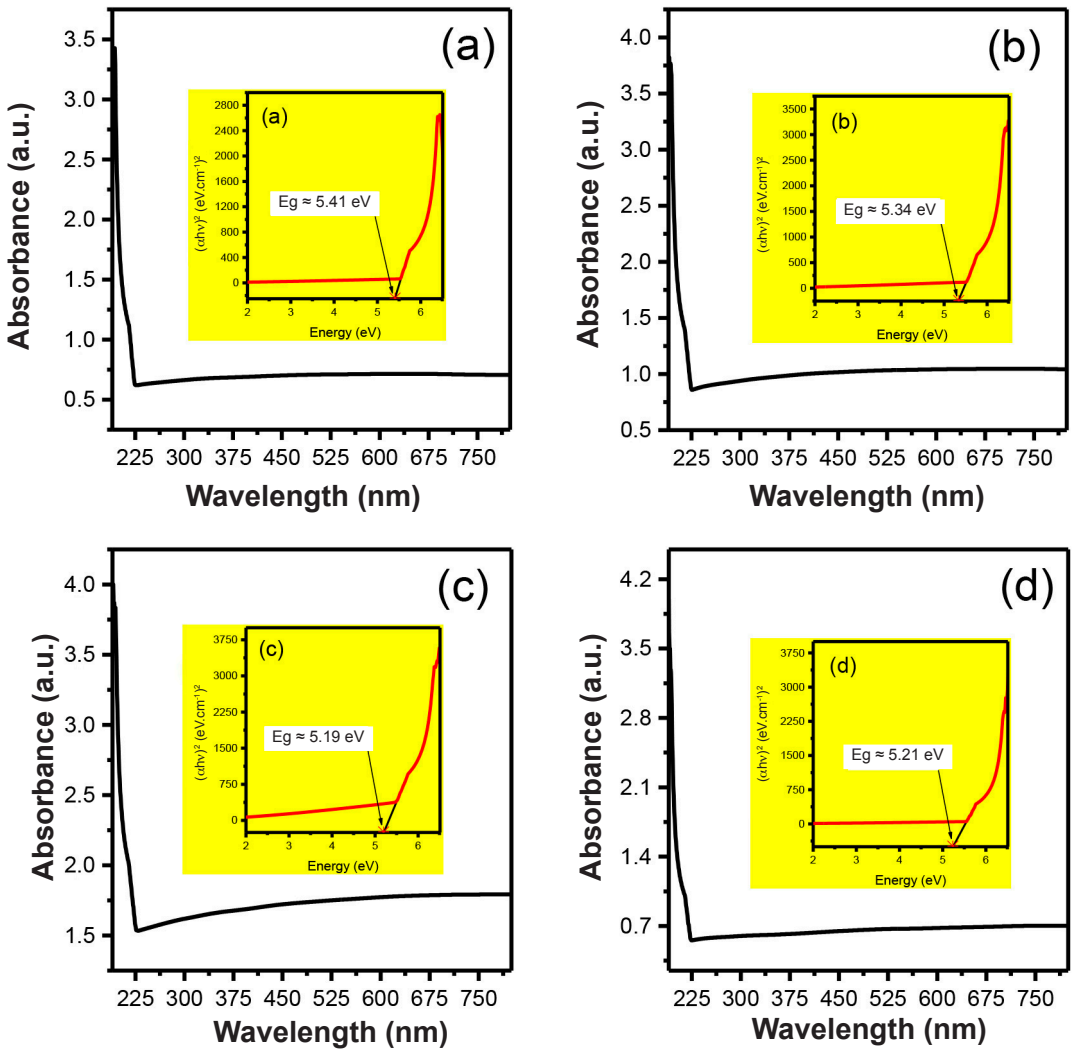

Figure 10: UV-vis absorption spectra of rhombohedral tricalcium phosphate samples calcined at 800 °C (a,b) and at 1000 °C (c,d)

light, probably due to oxygen deficiencies compared with hydroxyapatite [$Ca_5(PO_4)_3.(OH)_2$] that can have photocatalytic activity under UV light, due to the reported optical band gap energy of all samples varied greatly (E_g ~5.34 to ~5.41 eV, and ~5.19 to ~5.21 eV). However, the optical energy gap of the rhombohedral tricalcium phosphate sample tended to decrease when the calcination temperature increased from 800 to 1000 °C.

CONCLUSIONS

The sample of rhombohedral tricalcium phosphate in the hexagonal crystal structure prepared by a sol-gel route was influenced by the calcination temperature and was studied by several tests, such as FTIR, XRD, SEM-EDX, DSC-TGA, and UV-vis spectroscopy. The information of deficiencies of the hydroxyl functional group of -OH was shown by FTIR and this indicated the results of a tricalcium phosphate when calcination temperatures at 800 and 1000 °C were applied to this sample. The rhombohedral structure in the hexagonal crystal system of the sample was confirmed by XRD, where the Miller indices showed the rhombohedral lattice plane orientation at two points (011) and (111). The temperatures used at 800 and 1000 °C were confirmed by DSC-TGA and effectively influenced and made the sample of tricalcium phosphate with a stable structure in the rhombohedral system. The atomic ratio Ca/P ~1.5 of the rhombohedral tricalcium phosphate sample was found by EDX and its surface topography looked like white clouds using SEM. Finally, the optical energy gap of the rhombohedral tricalcium phosphate sample had quite large values of E_g ~5.34-5.41 eV, when calcined at 800 °C, and E_g ~5.19-5.21 eV, when calcined at 1000 °C. These results indicated that the optical band gap of the rhombohedral tricalcium phosphate sample tended to be wide and to decrease when the calcination temperature increased.

ACKNOWLEDGMENTS

We thank especially the Ministry of Research, Technology, and Higher Education of Indonesia for providing all support.

REFERENCES

[1] A.I. Ibrahim, N.R. Al-Hasani, V.P. Thompson, S. Deb, J.

Clin. Exp. Dent. **12**, 4 (2020) 317.
[2] A. Seifert, J. Groll, J. Weichhold, A.V. Boehm, F.A. Müller, U. Gbureck, Adv. Eng. Mater. **23**, 5 (2021) 1.
[3] N. Laohavisuti, B. Boonchom, W. Boonmee, K. Chaiseeda, S. Seesanong, Sci. Rep. **11**, 1 (2021) 1.
[4] W.M. Haynes, *Handbook of chemistry and physics*, 97th ed., CRC Press (2016) 121.
[5] K. Rubenis, S. Zemjane, J. Vecstaudza, J. Bitenieks, J. Locs. J. Eur. Ceram. Soc. **41**, 1 (2021) 912.
[6] S. Grasso, M. Biesuz, L. Zoli, G. Taveri, A.I. Duff, D. Ke, A. Jiang, M.J. Reece, Adv. Appl. Ceram. **119**, 3 (2020) 115.
[7] M. Yashima, A. Sakai, T. Kamiyama, A. Hoshikawa, J. Solid State Chem. **175**, 2 (2003) 272.
[8] H. Chaair, H. Labjar, O. Britel, Morphologie **101**, 334 (2017) 124.
[9] D. Moreno, F. Vargas, J. Ruiz, M.E. López, Bol. Soc. Esp. Ceram. V. **59**, 5 (2020) 2.
[10] T.V. Safronova, I.I. Selezneva, S.A. Tikhonova, A.S. Kiselev, G.A. Davydova, T.B. Shatalova, D.S. Larionov, J.V. Rau, Bioact. Mater. **5**, 2 (2020) 423.
[11] A.P. Periyasamy, M. Venkataraman, D. Kremenakova, J. Militky, Y. Zhou, Materials **13,** 8 (2020) 1838.
[12] G.J. Owens, R.K. Singh, F. Foroutan, M. Alqaysi, C. Han, C. Mahapatra, H. Kim, J.C. Knowles, Prog. Mater. Sci. **77** (2016) 1.
[13] P. Owczarz, M. Orczykowska, A. Rył, P. Ziółkowski, Food Chem. **271** (2019) 94.
[14] A.E. Danks, S.R. Hall, Z. Schnepp, Mater. Horizons **3**, 2 (2016) 91.
[15] M. Anugrahwati, M.D.P. Nasution, F.I. Fajarwati, J. Pijar Mipa **17**, 1 (2022) 73.
[16] E. Isparnadi, M. Hidayat, A. Aulanni'am, N. Permatasari, Int. J. Chemtech Res. **8**, 6 (2015) 718.
[17] R. Jing, A. Varveri, X. Liu, A. Scarpas, S. Erkens, Road Mater. Pavement Des. **22**, 5 (2019) 1.
[18] L. Ma, M. Li, S. Komasa, S. Yan, Y. Yang, M. Nishizaki, L. Chen, Y. Zeng, X. Wang, E. Yamamoto, S. Hontsu, Y. Hashimoto, J. Okazaki, Materials **15**, 6 (2022) 2306.
[19] Y. Tang, X. Qiu, X. Gong, Y. Tang, Acta Mater. Compos. Sin. **39**, 1 (2022) 169.
[20] Í.E.L. Viana, R.M. Lopes, F.R.O. Silva, N.B. Lima, A.C.C. Aranha, S. Feitosa, T. Scaramucci, J. Dent. **92** (2020) 103263.
[21] M. Zheng, D. Fan, X.K. Li, Q.B. Liu, J.B. Zhang, Key Eng. Mater. **373-374** (2008) 710.
[22] H. Zhang, S. Xu, Y. Xiong, R. Gao, X. Li, J. Mech. Eng. **55**, 15 (2019) 81.
[23] S.A. Silva, R.E.F.Q. Nogueira, J.M.C. Teixeira, J.S.V. Albuquerque, E.B. Duarte, Matéria **24**, 1 (2019) 1.
[24] T. Tariverdian, A. Behnamghader, P.B. Milan, H. Barzegar-Bafrooei, M. Mozafari, Ceram. Int. **45**, 11 (2019) 14029.
[25] T. Furihata, H. Miyaji, E. Nishida, A. Kato, S. Miyata, K. Shitomi, K. Mayumi, Y. Kanemoto, T. Sugaya, T. Akasaka, J. Biomed. Mater. Res. B Appl. Biomater. **108**, 7 (2020) 34632.
[26] M. Taherimehr, R. Bagheri, M. Taherimehr, Ceram. Int. **47**, 11 (2021) 15458.
[27] Y.M. Sahin, Z. Orman, S. Yucel, J. Aust. Ceram. Soc. **56**, 2 (2020) 477.
[28] D.H. Yang, M.S. Bae, L. Qiao, D.N. Heo, J.B. Lee, W.J. Lee, J.H. Park, D.W. Lee, Y. Hwang, I.K. Kwon, Macromol. Res. **20**, 7 (2012) 754.
[29] J.A.R. Pasqual, L.C. Freisleben, J.C. Colpo, J.R.J. Egea, L.A.L. dos Santos, V.C. de Sousa, J. Mater. Sci. Mater. Med. **32**, 4 (2021) 38.
[30] R. Bento, A. Gaddam, J.M.F. Ferreira, Materials **14**, 16 (2021) 4515.
[31] T.N.M. Bernards, M.J. van Bommel, E.W.J.L. Oomen, A.H. Boonstra, J. Non. Cryst. Solids **147-148** (1992) 13.
[32] O.E. Shapovalova, A.S. Drozdov, E.A. Bryushkova, M.I. Morozov, V.V. Vinogradov, Arab. J. Chem. **13**, 1 (2020) 1933.
[33] M.A. Almessiere, Y. Slimani, U. Kurtan, S. Guner, M. Sertkol, S.E. Shirsath, S. Akhtar, A. Baykal, I. Ercan, Ultrason. Sonochem. **58** (2019) 104638.
[34] A. Vilvanathaprabu, B. Ravikumar, J. Phys. Conf. Ser. **1644**, 1 (2020) 12034.
[35] P. Phatai, C.M. Futalan, S. Utara, P. Khemthong, S. Kamonwannasit, Results Phys. **10** (2018) 956.
[36] S. Kannan, F. Goetz-Neunhoeffer, J. Neubauer, A.H.S. Rebelo, P. Valério, J.M.F. Ferreira, J. Biomed. Mater. Res. B Appl. Biomater. **90**, 1 (2009) 31299.
[37] A.C.B. Jesus, J.R. de Jesus, R. Lima, K.O. Moura, J.M.A. Meneses, J.G.S. Duque, C. Meneses, Ceram. Int. **46**, 8 (2020) 11149.
[38] M. Horchani, A. Omri, A. Benali, M.S. Eddine, A. Tozri, E. Dhahri, M.P.F. Graça, M.A. Valente, B.F.O. Costa, S.K Jakka, J. Solid State Chem. **308** (2022) 122898.
[39] S.K. Sen, U.C. Barman, M.S. Manir, P. Mondal, S. Dutta, M. Paul, M.A.M. Chowdhury, M.A. Hakim, Adv. Nat. Sci. Nanosci. Nanotechnol. **11**, 2 (2020) 5004.
[40] N.W. Ashcroft, N.D. Mermin, *Solid state physics*, Rinehart Winston, New York (1976).
[41] D. Louër, J.P. Auffrédic, J.I. Langford, D. Ciosmak, J.C. Niepce, J. Appl. Crystallogr. **16**, 2 (1983) 183.
[42] D. Balzar, N. Audebrand, M.R. Daymond, A. Fitch, A. Hewat, J.I. Langford, A. Le Bail, D. Louër, O. Masson, C.N. McCowan, N.C. Popa, P.W. Stephens, B.H. Toby, J. Appl. Crystallogr. **37**, 6 (2004) 911.
[43] A.L.C.S. Nascimento, G.M.B. Parkes, G.P. Ashton, R.P. Fernandes, J.A. Teixeira, W.D.G. Nunes, M. Ionashiro, J. Anal. Appl. Pyrolysis **135** (2018) 67.
[44] M. Ciecińska, P. Goj, A. Stoch, P. Stoch, J. Therm. Anal. Calorim. **139**, 3 (2020) 1763.
[45] F.P.N. Inbanathan, P. Kumar, K. Dasari, R.S. Katiyar, J. Chen, W.M. Jadwisienczak, Materials **14**, 12 (2021) 3307.
[46] J.B. Coulter, D.P. Birnie, Phys. Status Solidi Basic Res. **255**, 3 (2018) 1700393.
[47] M. Sheik-Bahae, D.C. Hutchings, D.J. Hagan, E.W. Van Stryland, IEEE J. Quantum Electron. **27**, 6 (1991) 89946.
[48] S. Muhammady, Y. Kurniawan, M.A.K. Purbayanto, Y. Darma, Mater. Res. Express **5**, 6 (2018) 66303.
(Rec. 09/08/2022, Rev. 16/11/2022, 31/12/2022, Ac. 07/01/2023)